PCCP

Accepted Manuscript

ROYAL SOCIETY OF CHEMISTRY

www.rsc.org/pccp

Graphical Abstract (a picture and 20 to 30 words)

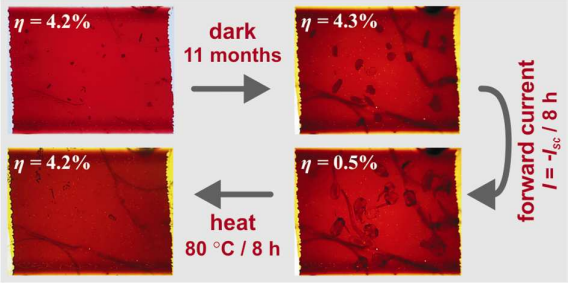

The efficiency recovery of dye-sensitized solar cell and crystal growth in cell stored in the dark, treated with a forward bias current and exposed to heat treatment.

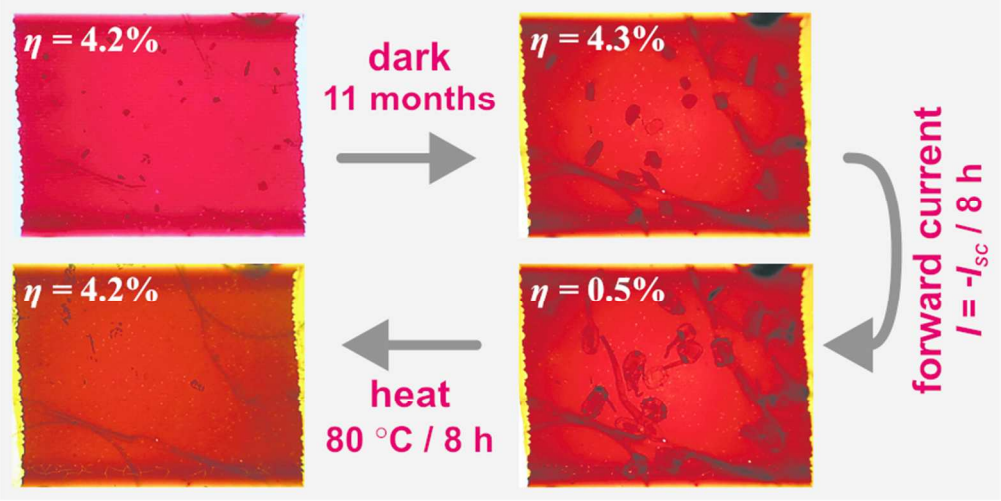

79x39mm (300 x 300 DPI)

Recovery of dye-sensitized solar cell's performance by heat treatment

Marko Berginc, Marko Topič, Urša Opara Krašovec
University of Ljubljana, Faculty of Electrical Engineering
Tržaška 25, SI-1000 Ljubljana, Slovenia
(E-mail: marko.berginc@fe.uni-lj.si)

Abstract:

The formation of iodine containing crystals with ageing in ionic liquid based dye-sensitized solar cells (DSSCs) containing an I_3^-/I^- redox couple has already been confirmed. In this report we show how the size of these crystals can reversibly change during operation and the effects this has on cell performance. We also show how heat treatment and applied forward and reverse current treatment influence crystal growth in the cell. Crystal growth was tracked using electroluminescence and transmittance imaging, while current-voltage characterization and electrical impedance spectroscopy was used to measure cell performance and follow the changes in I_3^- diffusion, charge transfer resistance, and recombinations occurring in the DSSCs. Results reveal that applying a reverse current to the DSSC leads to the rapid formation of H_2 bubbles while crystals grow rapidly when a forward current is applied. Additionally heat treatment at 80 °C can completely recover performance of a degraded cell showing visible defects and a large inhomogeneous active area.

1 Introduction

Dye-sensitized solar cells (DSSCs) have been extensively studied as a low-cost alternative to silicon solar cells[1,2]. Over the last two decades various materials including dyes and electrolyte components have been developed with the aim of improving conversion efficiency and cell stability. Despite this cell stability remains an issue[3-11]. Photovoltaics cells/modules must pass tests related to stability as specified in the IEC 61646 or IEC 61215 standards to qualify for the market. In addition solar cells are expected to pass specific industry-driven tests of which the most challenging for DSSC technology remains the light soaking test at 85 °C[5], while the thermal test at 85 °C in the dark and the light soaking test under full sunlight at 60 °C[6,12] are slightly less demanding.

Cell or PV module aging can be done both indoors starting with temporal stability testing in the dark at room temperature, albeit more usually under continuous accelerated conditions, or outdoors under location-specific and field-specific (year/season/day) conditions. Generally, regardless of the type of ageing, a progressive decrease in performance parameters *i.e.* short circuit current J_{SC}, open circuit voltage V_{OC} and, fill factor *FF* and conversion efficiency (η) is expected. This is not always the case and variations in these performance parameters occurs during ageing under different conditions[6,10,12-21], which at times can even recover the η of an aged cell at a certain stage. One example is the decrease in J_{SC} which accompanies an increase in *FF* due to reduced serial resistance losses[11]. Some variations that occur with ageing are more difficult to explain. For instance the increase in V_{OC}, which is thought to be a result of an upward shift of the TiO_2 Fermi level will decrease the J_{SC} due to reduced electron injection from the excited dye into the TiO_2[13,17]. A similar increase in V_{OC} and *FF* and a decrease in J_{SC} and η were also observed by Kim *et al.*[22] who periodically measured the performance of DSSCs stored in the dark for 43 days under standard test conditions (STC). The change in

performance was ascribed to the growth of dark coloured needle-shaped solid crystals on the TiO_2 layer appearing 10 days after fabrication[22]. Fourier transform infrared spectroscopy indicated that these crystals are related to dye becoming detached from the TiO_2 surface in the presence of guanidinium thiocyante in the electrolyte, since guanidine can react with water present in the cell to form ammonia - a dye desorbing agent[22]. Alternatively, Fischer *et al.*[23] found dark brown, almost black crystals in their DSSCs after one to two weeks. This occurred when *N*-methylbenzimidazole (MBI) was added to an I_3^-/I^- based electrolyte with *3*-methoxypropionitrile (MPN) as a solvent. The change in the colour of the electrolyte from dark brown to yellow-orange is indicative of a substantial amount of iodine-containing species leaving the liquid phase[23]. The authors proposed that MBI interacts with I_3^- ions in the electrolyte to form neutral and/or ionic complexes, such as $(MBI)_6(MBI\text{-}H^+)_2(I^-)(I_3^-)$, which has been confirmed by X-ray diffraction[23]. The crystals consisted of six neutral and two protonated MBI fragments while I^- and I_3^- anions balance the overall charge. The organic layers are separated by inorganic layers with alternating I^- and linear I_3^- anions forming infinite chains along the crystallographic *a*-axis[23].

In our previous studies we examined such crystals using the light-beam-induced current technique, transmittance imaging (TI) and electroluminescence (EL)[11,24,25]. These methods allowed us to study local defects[24]. Electroluminescence imaging demonstrated that short term ageing (irradiation ≤ 30 kWh/m^2) is associated with crystal growth in the electrolyte[25]. Under an open-circuit condition crystal growth increased both V_{OC} and η, while under a short-circuit condition crystal growth was more pronounced and a decrease in J_{SC}, V_{OC} and η were observed[25]. More recently we revealed that the dark crystals are introduced into the cells along with the electrolyte[11]. We also found that these crystals continued to grow when the cells were stored in the dark causing an increase in V_{OC} and a decrease in J_{SC}, but dissolved during the first 2 months of a 7 month outdoor ageing study (irradiation ≤ 909 kWh/m^2) regardless of the operating condition[11]. Interestingly, one large crystal typically grew during the final stage of ageing under open-circuit condition[11].

Because the formation/growth/dissolution of iodine based crystals in the electrolyte significantly influences the performance of DSSC we believe that it is important to understand the correlation between crystal development and cell performance. For this reason we have studied the effect of crystal development in cells that were (i) kept in the dark at standard room temperature (25 °C), (ii) exposed to heat, and (iii) subjected to either a forward or reverse current. Temperatures of 60 °C and 80 °C were chosen for heat treatment since cell temperature when outdoors can exceed 60 °C[8,26]. Reverse or forward currents proportional to the J_{SC} were also applied to non-illuminated cells to simulate shade conditions for cells connected in either series or parallel in a PV module. The EL and TI were used to track crystal development while current-voltage characterization (*I-V*) and electrical impedance spectroscopy (EIS) were used to correlate cell performance with processes occurring in the cells such as I_3^- diffusion, charge transfer resistance, and recombinations.

2 Experimental

2.1 Cell preparation

A fluorine-doped SnO_2 coated glass (TCO) with a sheet resistance of 8 Ω/□ was used for the front and back cell substrate. An optimized Pechini sol-gel TiO_2 paste (based on P25, Degussa, Germany)[27] was then applied to the surface of the front TCO glass substrate using the "*doctor blading*" technique. The TiO_2 layer was then sintered at 450 °C for 1 h before

being immersed for 12 h in an ethanol solution of a Ruthenium complex based dye N719 (Ru(2,2'bipyridyl-4,4'dicarboxylate)$_2$ (NCS)$_2$, Solaronix, Switzerland). For a counter electrode, platinum (thickness ~5 nm) was sputtered on a TCO glass substrate. The active and counter electrodes were then sealed using a 25 μm thick polymer foil frame (Surlyn, DuPont, USA). This also acts as a spacer between the two electrodes. As an electrolyte we used a binary ionic-liquid mixture of *1*-propyl-*3*-methyl-imidazolium iodide (Iolitec) and *1*-ethyl-*3*-methyl-imidazolium tetracyanoborate in a volume ratio 13:7 (Merck), with the addition of 0.5 M *N*-methylbenzimidazol, 0.1 M guanidinium thiocyanate and 0.2 M of I_2. This composition is considered the best binary ionic liquid electrolyte for DSSCs[28]. After injecting the electrolyte through two pre-drilled holes in the counter electrode the cells were sealed and stored in the dark for 24 h to allow for complete penetration of electrolyte into the pores of the TiO_2 layer. The size of the active area was 0.63 ± 0.05 cm^2.

2.2. Characterization

Cells under test were routinely characterized at different times according to Table 1. The *I-V* scan at STC, electroluminescent image (EL) and transmission image (TI) were always used for characterization. After initial characterization (phase a) the cells were stored in the dark at room temperature (RT, 25 °C) under an open-circuit condition for an initial resting period of 11 months (1st resting period). The cells were then treated as described in Table 1 (phase b). After each heat treatment (each time period and temperature) the cells were cooled down prior taking the *I-V* scan at STC. After phase b the cells were rested for a second time (2nd resting period) in the dark at RT under an open-circuit condition for a further 9 months. After resting the cells were then characterized again (phase c1) before being heated at 80 °C for 8 h in the dark under an open-circuit condition (phase c2). During heat treatment the cells were stored in the dark at open-circuit condition. A series of reference cells were also stored in the dark at RT.

I-V scan

I-V characterization was performed using an Oriel Class ABA solar simulator (Newport, USA) equipped with a 1.5G air mass filter, the spectrum of which closely matches the required AM1.5 spectrum. In accordance with the IEC60904-3 standard the short-circuit current mismatch parameter was calculated and in conjunction with a calibrated c-Si reference solar cell covered with a KG5 glass filter, the level of standard illumination (1 sun, 1000 W/m^2) was determined. The cells were also masked to leave only the active area of the cell exposed. This is considered the most rigorous condition regarding cell efficiency. *I-V* characteristics of the cells were then measured using a Keithley 238 source meter by applying a voltage and measuring the current. The cells were scanned stepwise (10 mV) from 0 V (short-circuit condition) to 0.9 V (beyond V_{OC}). During the measurement the cell temperature was always stabilized to 25 °C using cooling/heating setup based on Peltier element.

EL

The electroluminescence measurement (EL) is a powerful method to observe spatial defects in solar cells. When a current (usually equal to short-circuit current) is applied to the solar cell in the dark the cell radiates the IR photons which are detected with an imaging device. In our setup we used a CCD camera (FLI, MLx285, USA), which utilizes a low noise monochromatic 1.5 megapixel CCD sensor with improved *EQE* in the NIR region and a cooling system to minimize background noise. The camera was also equipped with a 12 mm colour corrected Vis-NIR lens with a wide focus range. During measurements the camera, the camera lens and the cell were housed in a custom-built dark enclosure. The working electrode was oriented towards the camera. A laboratory power supply was then used to forward bias

the cells with a short-circuit current previously measured under STC. The CCD array was kept at 0 °C and an exposure time set to 300 s. Optical and spatial constraints meant that only 600×600 pixels were effectively used for image acquisition.

TI

The transmittance image (TI) is a method to observe visual spatial defects. The semi-transparent DSSC is backlit using a diffused white light emitting diode and the photo of the cell is then acquired using a 2-mega pixel digital microscope camera DigiMicro 2.0 Scale (DNT, Germany).

EIS

Electrical impedance spectroscopy (EIS) was performed using a potentiostat (Zahner Elektrik IM6e, Germany) with Thales software in a 10 mHz - 1 MHz frequency range with an AC amplitude of 5 mV. The illuminated cells (1000 W/m^2) were kept under open-circuit conditions. The EIS spectra were analysed according to the procedure described in the literature[29]. More information about the analysis and a typical Nyquist plot with denoted parameters can be found in the Electronic Supplementary Information - ESI (Fig. S4).

Table 1: The sequence of methods used to characterise the DSSCs (*I-V* current-voltage characteristics, EL electroluminesce, TI transmittance imaging). The reference cell (cell 1) was stored at RT while the cells 2 and 3 were heat treated at 60 °C and 80 °C, respectively. A reverse and forward bias current was then applied to cells 4 and 5, respectively.

phase	**heat treatment** cell 1 / cell 2 / cell 3	**reverse bias current** cell 4	**forward bias current** cell 5
a	*I-V*, EL, TI	*I-V*, EL, TI	*I-V*, EL, TI
	11 months / dark, RT	**11 months / dark, RT**	**11 months / dark, RT**
b	*I-V*, EL, TI	*I-V*, EL, TI	*I-V*, EL, TI
	5 min at RT/60 °C/80 °C	5 min 30 s at 0.2×J_{SC}, TI	6 h 40 min at –J_{SC}, TI
	I-V, EL, TI	6 h 40 min at J_{SC}, TI	17 h 30 min at –2×J_{SC}, TI
	10 min at RT/60 °C/80 °C	18 h at 2×J_{SC}, TI	66 h at –2×J_{SC}, TI
	I-V, EL, TI	*I-V*, EL, TI	*I-V*, EL, TI
	15 min at RT/60 °C/80 °C	1 h at 80 °C	1 h at 80 °C
	I-V, EL, TI	*I-V*, EL, TI	*I-V*, EL, TI
	30 min at RT/60 °C/80 °C	-	-
	I-V, EL, TI	-	-
	60 min at RT/60 °C/80 °C	-	-
	I-V, EL, TI	-	-
	2 h at RT/60 °C/80 °C	-	-
	I-V, EL, TI	-	-
	2 h at RT/60 °C/80 °C	-	-
	I-V, EL, TI	-	-
	9 months / dark, RT	**9 months / dark, RT***	**9 months / dark, RT***
c1	*I-V*, EL, TI	*I-V*, EL, TI*	*I-V*, EL, TI*
	8 h at 80 °C	**8 h at 80 °C***	**8 h at 80 °C***
c2	*I-V*, EL, TI	*I-V*, EL, TI*	*I-V*, EL, TI*

* not shown

3 Results and discussion

3.1 Heat treatment

Electroluminescent images and performance parameters (J_{SC}, V_{OC}, *FF* and η) of the reference cell (cell 1) and the cells heat treated at 60 °C (cell 2) and 80 °C (cell 3) are presented in Figs. 1 and 2, respectively. For the reference cell the same measurement protocol and timeline as for the heat treated cells was applied (see Experimental). This means that any changes observed in cell performance and crystal development in the reference cell is a result of repeated *I-V* scans and EL image acquisitions. Herein, only the progress of a typical DSSC for each temperature is presented. The performance parameters of these cells and an additional cell at each temperature together with TI and EL images with additional intermediate snapshots are given in the ESI (Table S1 and Figs. S2 and S3, respectively).

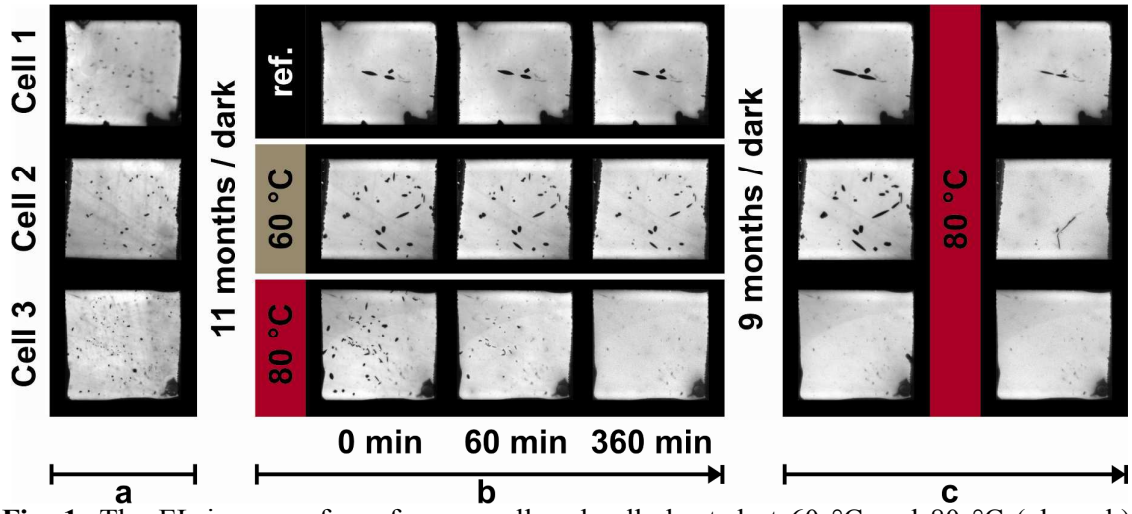

Fig. 1: The EL images of a reference cell and cells heated at 60 °C and 80 °C (phase b). Additionally EL of the cells before 1st resting period (phase a), after 2nd resting period and after additional heat treatment at 80 °C for 8 h (phase c) are given. More frequent snapshot and EL images of additional cells are given in Fig. S2 in the ESI.

Phase a → phase b

The results show that after cell fabrication (phase a) all the cells had small inactive spots comprised of iodine containing crystals (Fig. 1). These crystals were already formed in the electrolyte and were introduced into the cells along with the electrolyte during cell fabrication[11,24,25]. During the 1st resting period the crystals continued to grow (Fig. 1) resulting in a reduction in the concentration of tri-iodine, $[I_3^-]$, in the electrolyte. This is reflected by a decrease in J_{SC} (approx. 1 mA/cm^2) and an increase in the V_{OC} (approx. 40 mV) after the 1st resting period (Fig. 2) and agreeing with Kim *et al.*[22]. We also observed a small increase in the *FF,* which is probably associated with reduced serial resistance losses due to a reduced J_{SC}. In all three cases, the increase in V_{OC} and *FF* overcome the decrease in J_{SC} resulting in an increase in η after the first resting period.

Phase b

Our results show that the crystals in the reference cell (cell 1) were not affected by either continuous *I-V* characterization or EL imaging (phase b in Fig. 1). Continuous measurement did observably cause the J_{SC} to initially increase, but after a few measurements it remained unchanged. This is thought to be related to the reactivation of the counter electrode by repeated *I-V* measurements after a long resting period. There was also a negligible increase in

V_{OC} while the *FF* initially decreased but then remained constant. This decrease in *FF* is associated with the increase in the J_{SC}. As a result, η remained stable. Taking into account all our observations we find that repeated *I-V* measurements and EL imaging does not significantly affect either cell performance or the size of the crystals in cell 1.

Heat treatment at 60 °C (cell 2) and 80 °C (cell 3) affects both cell performance and crystal size. The crystals in cells 2 and 3 gradually dissolve during heat treatment (Fig. 1) with dissolution being significantly faster at 80 °C compared to 60 °C. Our EL measurements show that the crystals completely disappeared in the cells exposed to 80 °C for 4 h (ESI, Fig. S2). When exposed to 60 °C for 6 h the crystals did not disappear but were significantly reduced in size (Fig. 1). The dissolution of the crystals also affects cell performance. The J_{SC} of the cell exposed to 60 °C and cell exposed to 80 °C logarithmically increased with time. This initial increase in the J_{SC} may, in part, be related to the reactivation of the DSSC due to repeated *I-V* measurements as observed for the reference cell. Nevertheless, a more intense and rapid increase in J_{SC} is observed when the cells were heated at 80 °C (cell 3) and is related to the rapid dissolution of the crystals. The J_{SC} of cell 3 after being heated for 6 h (phase b) exceeds the initial J_{SC} (phase a), while remaining below the initial J_{SC} in the case of cell 2. The J_{SC} of cell 2 (treated at 60 °C) monotonically increased with time, whereas J_{SC} decreases during the final 2 h of heat treatment at 80 °C (cell 3). Similar observations were found for the equally treated cell 3a (Table S1 in the ESI). We believe that this decrease in J_{SC} is probably related to a degradation of the electrolyte, an observation affirmed by electrical impedance spectroscopy (see below).

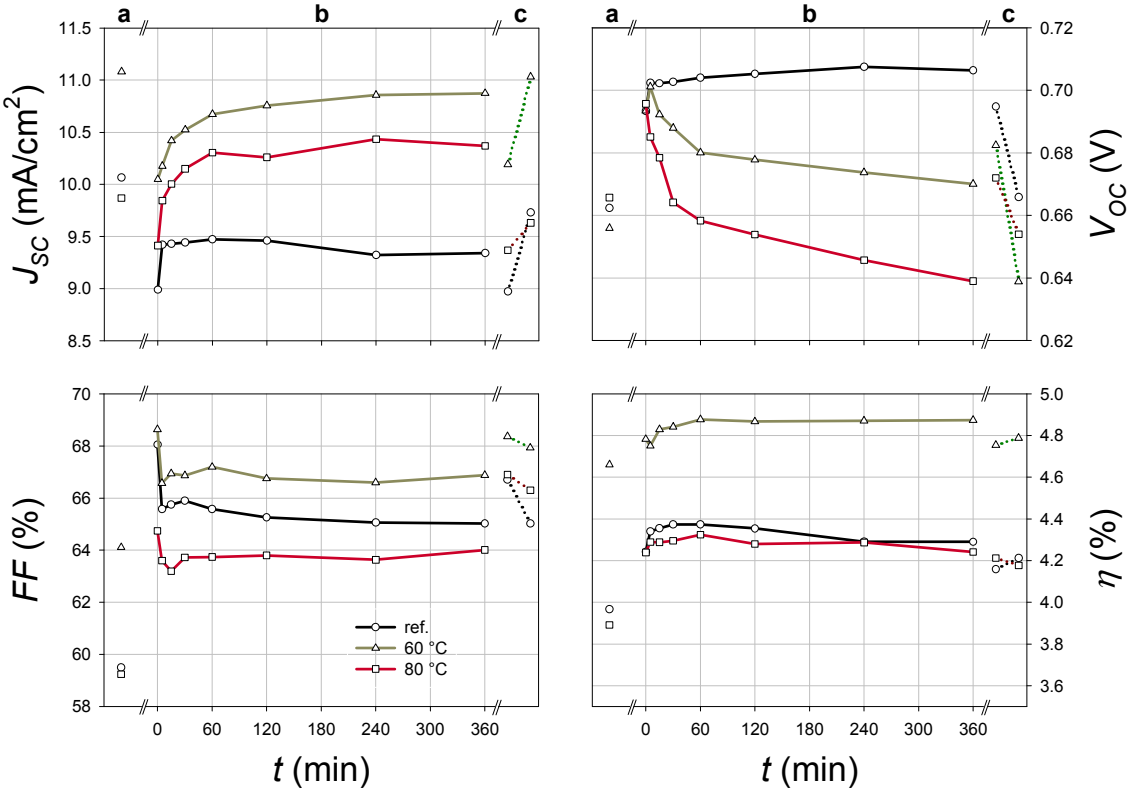

Fig. 2: Performance parameters: J_{SC}, V_{OC}, *FF* and η, of the reference cell and cells heated at 60 °C or 80 °C for different time period (phase b). Additionally the performances that were measured 11 months prior to heat treatment (phase a), 9 months after the treatment and after additional heat treatment at 80 °C for 8 h (phase c) are also given.

The dissolution of the iodine containing crystals in cell 2 and 3 also lead to an increase [I_3^-] in the electrolyte, which shifted the redox potential of the electrolyte upward and stimulates recombinations. Both mechanisms decrease the V_{OC}, which is confirmed by the exponential decrease in V_{OC} with time (Fig. 2). According to expectations the observed reduction in V_{OC} is faster and more intensive in the case of cell 3. The *FF* sharply decreases during the first 30 min but then remains unaffected. This is a probable result of serial resistance losses due to the sudden initial increase in the J_{SC}. With the exception of a minor initial fluctuation, η remained stable during heat treatment at both 60 °C and 80 °C, although significant variations in J_{SC} and V_{OC} were observed (Fig. 2).

Phase b → phase c

After heat treatment the cells were rested in the dark for a further 9 months at 25 °C. During this 2nd resting period, the crystals that were present after heat treatment continued to grow (cell 1 and cell 2), whereas in cell 3, where the crystals had completely disappeared, EL measurements revealed the active area to have remained unchanged. Previously, crystal growth had resulted in an increased V_{OC} and decreased the J_{SC} (cell 2) but in this case the J_{SC} and V_{OC} of the reference (cell 1) decreased slightly albeit an increase in V_{OC} would have been expected due to crystal growth. The reason for this remains unknown. The *FF* of all the cells increased and is probably related to a decrease in the J_{SC}. A small decrease in η was also observed. Cell 3 followed the same trend although no crystal formation was observed during this period. This behaviour is difficult to explain but could be related to either cell degradation that occurred during the final 2 h of heat treatment at 80 °C or that any crystals present were too small to be detected with EL imaging. Interestingly, for any individual cell, J_{SC} remained constant after the 1st and 2nd resting period while in between, due to the different heat treatments, large variations were observed.

Phase c

Finally, all the cells were exposed to 80 °C for 8 h. The resultant EL images revealed that during heat treatment the crystals had almost completely dissolved in cell 1 and cell 2 leaving only negligible residues. Cell 3 had remained homogeneous. According to expectations all cells showed an increase in J_{SC}, a decrease in V_{OC} and a decrease in *FF*. Unexpectedly, the performance of the cell 3 had changed in a similar manner to cells 1 and 2 but the magnitude of change was smaller. The opposite behaviour was observed for η, which increased slightly for the reference cells (cell 1 and 1a; see Table S1 in the ESI), increased or decreased for cells 2 and 2a, and decreased for the cells 3 and 3a.

The electrolyte used in our study contained both guanidinium thiocyanate and the *N*-methylbenzimidazol which means that the crystals could originate from either dye desorption as proposed by Kim *et al.*[22] or are crystals of $(MBI)_6(MBI\text{-}H^+)_2(I^-)(I_3^-)$ as proposed by Fischer *et al.*[23]. In our case, crystallization is best explained by the formation of a iodine containing crystal such as an $(MBI)_6(MBI\text{-}H^+)_2(I^-)(I_3^-)$ complex[23]. First, the crystals were introduced into the cells along with the electrolyte (phase a) and second, the J_{SC} decreased and the V_{OC} increased as the crystals grew. This can be correlated to the variation in [I_3^-] but cannot be explained by dye desorption, since the presence of an undyed TiO_2 surface acting as a strong recombination centre would cause a decrease in V_{OC}. Finally, heat treatment demonstrated the reversibility of the process, which is related to crystal growth/dissolution - a fact that supports the presence of iodine containing crystals. After heat treatment the V_{OC} decreased while J_{SC} increased possibly to its highest recorded value (cell 3, Fig. 2). Such an increase would be unlikely if crystal formation was a result of dye desorption.

EIS

Figure 3 shows the EIS spectra of a typical illuminated cell under an open-circuit condition measured before and after being heated to 80 °C for 4, 12 and 20 h. The procedure on how to extract parameters from the EIS scans[29] together with the obtained values for this cell and two additional identical cells are given Table S2 in the ESI.

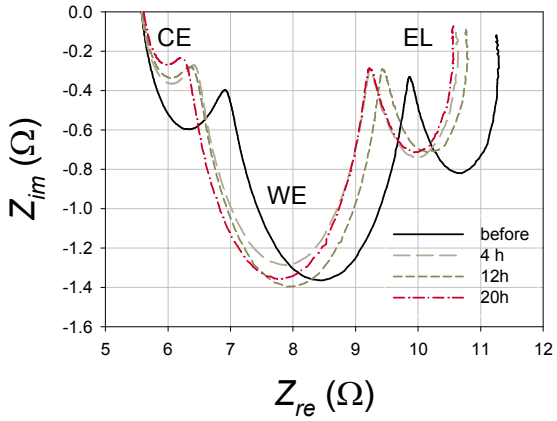

Fig. 3: Nyquist plots of the EIS spectra of a typical illuminated DSSC under open-circuit conditions. The spectra were measured before and after being heated at 80 °C for 4, 12 and 20 h. The high, central and low frequency semicircles relate to processes at the counter electrode (CE), working electrode (WE) and in electrolyte (EL), respectively.

A typical Nyquist plot of the EIS spectrum consists of three semicircles each measured in a different frequency range; a high frequency semicircle describes the processes at the counter electrode (CE), a central semicircle for the working electrode (WE), while a semicircle measured at low frequency range shows the diffusion of I_3^- in the electrolyte (EL). The results show that the series resistance R_s remained unaffected by heat treatment, whereas there is an initial sharp decrease followed by a gradual decrease in the charge transfer resistance R_{ct}. Two mechanisms can explain this decrease: 1) crystal dissolution and 2) a cleaning of the Pt layer on the counter electrode. Initially, it appears that not only the Pt but mostly a too low initial $[I_3^-]$ in the electrolyte determine the R_{ct}. After 4 h of heat treatment the $[I_3^-]$ increases sharply reducing the R_{ct} to that extent that only the Pt layer limits the charge transfer at the counter electrode. Presumably, prolonged heat treatment causes a continuous increase in the $[I_3^-]$. Because there is a sufficient amount of I_3^- for the charge transfer to occur at the counter electrode the R_{ct} does not further decrease. A cleaning of the Pt layer on the counter electrode during heat treatment is also possible causing R_{ct} to gradually decrease[11]. The effective recombination constant for the electrons k_{eff} is proportional to the angular frequency $\omega_2 = 2\pi k_{eff}$ where the central semicircle of the impedance spectra (Fig. 3) reaches its lowest imaginary part. The k_{eff} linearly increases with time until 12 h, where after prolonged treatment up to 20 h reduced the k_{eff} by 4.5%. This initial linear increase in the k_{eff} supports our hypothesis that the $[I_3^-]$ increases when the iodine containing crystals are dissolved. Alternatively, cell degradation might be responsible for the decrease in the k_{eff} after prolonged heat treatment. This is in accordance with our previous findings where an irreversible loss of $[I_3^-]$ was observed after ageing[11]. The diffusion coefficient of the I_3^- ions in the electrolyte D_I decreases with heat treatment up to 12 h and although D_I would be expected to be independent of the $[I_3^-]$, the higher $[I_3^-]$ in the electrolyte hampers the $[I_3^-]$ transport from the working to the counter electrode. Additionally, higher $[I_3^-]$ promotes the recombinations of

electrons with I_3^- ions and both effects will reduce D_I upon prolongation of heat treatment. After 12 h the D_I increased which is potentially another consequence of the irreversible loss of the [I_3^-] due to cell degradation.

The charge transfer resistance related to the recombination of the electrons R_k, resistance of diffusion of the I_3^- ions in the electrolyte R_d, and, the peak frequency of the semicircle in a high frequency range (ω_I) that is related to capacitance at the counter electrode are difficult to explain since they do not give direct insight into the processes taking place in the cells and do not have a significant effect on the performance.

3.2 Reverse and forward current treatment

Cells 4 and 5 were connected to a reverse and forward bias current, respectively, in the dark. The flows of the electrons and I_3^-/I^- ions are presented in Fig. 4 (left). The values of the reverse and forward bias currents (in relation to the J_{SC} measured under STC) are illustrated as dots on a typical dark *I-V* characteristic of a DSSC (Fig. 4, right).

The reverse bias was applied to cell 4. In this case the flow of the electrons and ions is the same as under normal operation under illumination, *i.e.* the applied current is positive. Since the current was applied in the dark, the voltage on the cell was negative. This condition would generally occur in a shaded cell that is connected in serial with others in a PV module. Alternatively, the electrons and ions flow in the opposite direction when a forward bias current was applied, *i.e.* the applied current is negative, while the voltage on the cell becomes positive (Fig. 4). A similar situation will occur in a shaded cell connected in parallel with the others in a PV module, *i.e.* the shaded cell would perceive a fixed voltage from the illuminated cells.

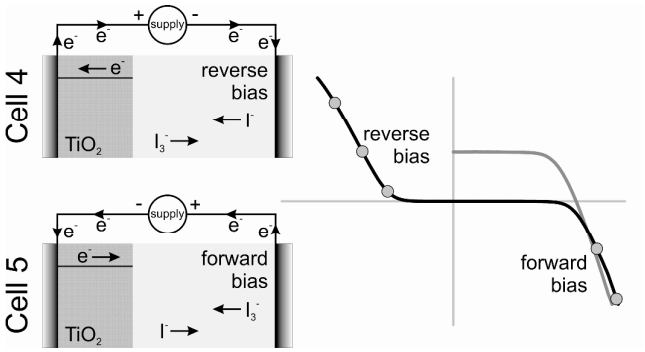

Fig. 4: The flow of the electrons in the DSSCs in the dark under reverse (top left) or forward bias current (bottom left). The graph (right) shows both a typical dark *I-V* characteristic of the DSSC and the values of the reverse and forward bias currents applied to the cells 4 and 5, respectively.

Figure 5 shows EL images of cells 4 and 5 measured after the following: fabrication (phase a), after 1st resting period, after applying reverse or forward current treatment, and after heat treatment at 80 °C for 1 h. Table 2 gathers the performance parameters: J_{SC}, V_{OC}, *FF* and η, measured under STC at equivalent stages. All stages of ageing including the more frequent TI snapshots during reverse or forward current treatment are shown in Fig. S6 in the ESI. Additionally, a movie is given in the ESI which demonstrates the accelerated evolution of spatial defects (formation of bubbles and crystal growth) under reverse and forward current treatment.

Phase a → phase b

Keeping these cells in the dark at 25 °C leads to the same conclusions as already observed for the cells examined in Section 3.1 (Figs. 1 and 2) *i.e.*, crystal growth during the resting period decreases the $[I_3^-]$ in the electrolyte therefore J_{SC} decreased significantly while V_{OC}, FF and η increased.

Table 2: The performance parameters (J_{SC}, V_{OC}, FF and η) of cells 4 and 5 measured under STC immediately after the fabrication (phase a), after 1st resting period (*i.e.* before current treatment), after reverse (cell 4) or forward (cell 5) current treatment, and finally after heat treatment at 80 °C for 1 h.

cell	time	J_{SC} (mA/cm^2)	V_{OC} (V)	FF (%)	η (%)
cell 4 (reverse)	fresh	9.74	0.664	56.2	3.63
	1st resting period	7.52	0.758	70.7	4.03
	reverse current treat.	0.00	0.007	0.0	0.00
	1 h at 80 °C	0.08	0.254	21.2	0.01
cell 5 (forward)	fresh	10.17	0.658	62.4	4.18
	1st resting period	9.37	0.695	65.8	4.29
	forward current treat. (1st meas.)	1.90	0.605	45.5	0.52
	forward current treat. (12th meas.)	6.95	0.628	54.7	2.39
	1 h at 80 °C	10.64	0.630	62.1	4.16

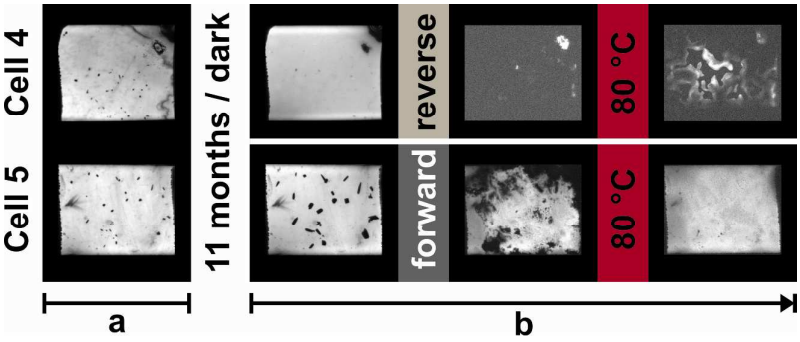

Fig. 5: The EL images taken after the fabrication (phase a), after 1st resting period (*i.e.* before current treatment), after reverse (cell 4) or forward (cell 5) current treatment and finally after the heat treatment at 80 °C for 1 h. All stages of ageing including the more frequent TI snapshots during both reverse and forward current treatment are presented in Fig. S6 in the ESI.

Phase b

Reverse current treatment

After the 1st resting period a reverse current (Fig. 4) was applied to the non-illuminated cell 4. After applying a constant current equal to $0.2\times J_{SC}$ for 5.5 min bubbles appeared after only a few seconds (Fig. 6; for more details see the movie and Fig. S6 in the ESI). These small bubbles then combined to form a few large bubbles. Applying a reverse current equal to the J_{SC} for 6.66 h resulted in a gradual decrease in bubble size and dye molecules to become detached from the TiO_2 surface. Finally, a current equal to $2\times J_{SC}$ was applied for a further 18 h. Initially a few large bubbles appeared, but soon after the cell became severely damaged.

The active area became very inhomogeneous and covered with bright and dark spots moving in the active area/electrolyte. During all three stages when a reverse current was applied the absolute value of the reverse bias voltage increased, *i.e.* the voltage across the cell became more negative, indicating a likely decrease in the $[I_3^-]$, which is in agreement with Mastroianni *et al.*[30,31].

The formation of bubbles and/or detachment of the dye molecules under reverse bias have already been observed[30-32]. Figgemeier *et al.*[32] observed the formation of oxygen and/or hydrogen bubbles when water entered a cell while Mastroianni *et al.*[30,31] observed a rapid degradation of DSSCs accompanied by dye detachment, evolution of gas inside the cell, and cell breakdown after applying voltages more negative than –1.65V. They found that the bubbles have an electrolysis-dependent origin and form at the Pt/electrolyte interface where I_2 reacts with residual H_2O, which in turn creates hydrogen bubbles[30]. They also observed that long bias stresses retain the dye in its oxidized state for a prolonged period of time making it more probable that it can suffer destructive reactions and irreversible degradations involving ligand oxidation, thiocyanate (SCN^-) detachment, and binding between SCN^- and impurities (such as H_2O/OH^-) or I^-/I_3^- ions[30].

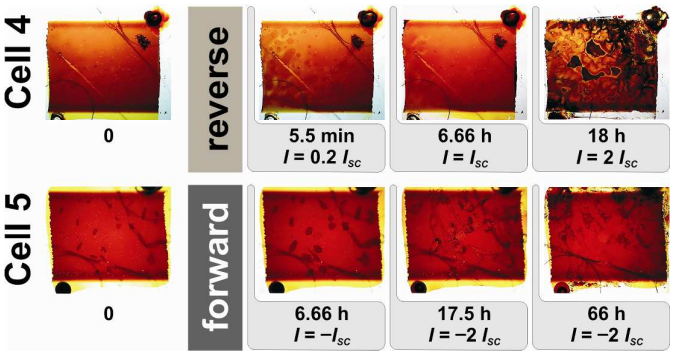

Fig. 6: The transmittance images (TI) before and after exposure to reverse (cell 4) or forward current treatment (cell 5).

Our results show that an applied reverse current significantly reduces cell performance. All performance parameters of cell 4 became virtually zero (Table 2). Such severe damage was also observed using EL which revealed that cell 4 was inactive (Fig. 5). After the reverse bias current treatment, cell 4 was then heated at 80 °C for 1 h. The virtual TI homogeneity of the cell (Figs. 6 and S6), the intensity of the EL response (Fig. 5), and the performance parameters (Table 2) improved but major defects remained such that heat treatment did not have a restorative effect. The cell was then rested for a 2nd resting period. Measurements were taken before and after an additional heat treatment at 80 °C for 8 h. Results show that cell performance parameters had improved during the 2nd resting period and partly during a further heat treatment but overall cell performance remained low (J_{SC}=0.11 mA/cm^2, V_{OC}=0.434 V, *FF*=33.7% and η=0.02%). Both defects and inhomogeneities were clearly observable by TI and EL (not shown here).

Forward current treatment

A forward bias current treatment was applied to the non-illuminated cell 5 after the 1st resting period (Figs. 5 and 6). First, a current equal to $-J_{SC}$ was applied to the cell for 6.66 h. During this period crystal growth was extremely fast when the current was applied and the area

covered by the crystals almost doubled in size after the first 6.66 h (Figure 6; see also movie and Fig. S6 in the ESI). We then applied a current equal to $-2\times J_{SC}$ for 17.5 h. The crystals rapidly grew out in all directions in a dendritic pattern. The colour of the crystals also became brighter. Finally the same current was applied for a further 66 h during which a similar phenomenon, albeit more gradual one, was observed. Then at the 59th h a strong collapse of electrolyte occurred introducing a major inhomogeneity in the cell. During all stages the value of the forward bias voltage also increased, indicative of a reduction in the $[I_3^-]$.

The breakdown of the cell that occurred after the forward bias current treatment was also observed by EL (Fig. 5). The active area of the cell also became inhomogeneous and covered with large inactive dark spots. In addition, performance parameters and especially the J_{SC} decreased significantly (Table 2), *i.e.,* η was reduced from 4.29% to 0.52% (88% relatively). Repeating *I-V* measurement gradually increased cell performance, which stabilized after 12 measurements. The value of η (2.39%), remained below 4.29% measured before applying a forward bias current.

After heating cell 5 at 80 °C for 1 h the cell's active area became homogeneous (Fig. 5), which implies an extensive restoration of cell performance. The J_{SC} reached its highest value while V_{OC} remained below its initial value (Table 2). Interestingly *FF* and η were practically the same as initially measured, which demonstrates the restorative effect of heat treatment on the performance of the DSSCs. After the 2nd resting period (not shown here) several small crystals had reappeared, which was also observed with TI and EL. The *I-V* measurements reveal a decrease in J_{SC} while *FF* and V_{OC} increased (J_{SC}=9.87 mA/cm^2, V_{OC}=0.655 V, *FF*=66.0%). Surprisingly, η reached 4.27% equalling the maximal value measured prior to applying a forward bias current. After heating cell 5 at 80 °C for a further 8 h (not shown here) the crystals dissolved and J_{SC} increased and V_{OC} decreased due to the higher $[I_3^-]$. In addition, *FF* decreased due to increasing serial resistance losses while η remained the same (J_{SC}=10.33 mA/cm^2, V_{OC}=0.630 V, *FF*=65.6%, η=4.27%).

4 Conclusions

Electroluminescent imaging and TI were successfully used to track the development of iodide containing crystals in ionic liquid based DSSC with a I_3^-/I^- redox couple that had been (i) stored in the dark, (iii) heat treated at 60 °C or 80 °C since cell temperature outdoors could easily exceed 60 °C, and (iii) exposed to reverse and forward current treatment in the dark to simulate a shaded cell connected in either series or parallel in a PV module. This study confirms that crystal growth occurs in cells stored in the dark for a significant period of time (9 - 11 months) and that heat treatment at both 60 °C and 80 °C leads to their dissolution.

I-V characterization confirmed that the presence of these crystals significantly influences the performance of the DSSCs. The formation/growth of the crystals is associated with a decrease in $[I_3^-]$ in the electrolyte which causes a decrease in J_{SC} and an increase in V_{OC}, while the opposite behaviour is observed when the crystals dissolved. Interestingly, the crystals do not reappear even after a resting period of 9 months if they had been completely removed by heat treatment. Our observations supports the theory that in the electrolyte the additive *N*-methylbenzimidazole reacts with iodine forming iodine containing crystals such as $(MBI)_6(MBI\text{-}H^+)_2(I^-)(I_3^-)$ complex.

In general, repeated *I-V* measurements under standard test conditions do not influence crystal growth. Applying a reverse current to the DSSC leads to the rapid formation of H_2 bubbles and detachment of the dye molecules from the TiO_2 surface which results in the irreversible breakdown of the cell. When a forward current is applied crystals growth is rapid and cell performance decreases by 88%. In this case repeated *I-V* measurements and especially a heat treatment at 80 °C for 1 h can restore cell performance showing a strong restorative effect of the heat treatment although the visible defects and strongly inhomogeneous active area caused a significant loss of the cell's performance in a first place. On the findings of our study heat treating DSSCs at 80 °C should be used to either initially stabilize or restore an I_3^-/I^- redox couple based electrolyte and in turn cell performance.

Acknowledgement

The authors would like to thank Marko Jankovec for his support in characterization of dye-sensitized solar cells. Mateja Hočevar is acknowledged for TiO_2 paste and electrolyte preparation and Jože Stepan for his help in fabricating the cells. Dr. David Heath is gratefully acknowledged for all his advices and for reading the manuscript. M.B. would like to acknowledge the Slovenian Research Agency (contract number Z2-4189-1538) for funding this study. The work was also partially funded by the Slovenian Research Agency under the P2-0197 program.

References

1 B. O'Regan, M. Grätzel, *Nature*, 1991, **353**, 737–740.
2 M. Grätzel, K. Kalyanasundaram, *Current Science*, 1994, **66**, 706–714.
3 A.G. Kontos, T. Stergiopoulos, V. Likodimos, D. Milliken, H. Desilvesto, G. Tulloch, P. Falaras, *The Journal of Physical Chemistry C*, 2013, **117**, 8636–8646.
4 N. Jiang, T. Sumitomo, T. Lee, A. Pellaroque, O. Bellon, D. Milliken, H. Desilvestro, *Solar Energy Materials & Solar Cells*, 2013, **119**, 36–50.
5 M.I. Asghar, K. Miettunen, J. Halme, P. Vahermaa, M. Toivola, K. Aitola, P. Lund, *Energy & Environmental Science*, 2010, **3**, 418–426.
6 R. Harikisun, H. Desilvestro, *Solar Energy*, 2011, **85**, 1179–1188.
7 L. Ciammaruchi, S. Penna, A. Reale, T.M. Brown, A. Di Carlo, *Microelectronics Reliability*, 2013, **53**, 279–281.
8] S. Mastroianni, A. Lanuti, S. Penna, A. Reale, T.M. Brown, A. Di Carlo, F. Decker, *ChemPhysChem: a European journal of chemical physics and physical chemistry*, 2012, **13**, 2925–2936.
9 A. Listorti, C. Creager, P. Sommeling, J. Kroon, E. Palomares, A. Fornelli, B. Breen, P.R.F. Barnes, J.R. Durrant, C. Lawa, B. O'Regan, *Energy & Environmental Science*, 2011, **4**, 3494–3501.
10 K. Zhu, S.-R. Jang, A.J. Frank, *Energy & Environmental Science*, 2012, **5**, 9492–9495.
11 M. Berginc, U. Opara Krašovec, M. Topič, *Solar Energy Materials & Solar Cells*, 2014, **120**, 491–499.
12 H. Pettersson, T. Gruszecki, C. Schnetz, M. Streit, Y. Xu, L. Sun, M.Gorlov, L. Kloo, G. Boschloo, L. Häggman, A. Hagfeldt, *Progress in Photovoltaics: Research and Applications*, 2010, **18**, 340–345.
13 S.H. Seo, S.Y. Kim, B.-K. Koo, S.-I. Cha, D.Y. Lee, *Langmuir: the ACS journal of surfaces and colloids*, 2010, **26**, 10341–10346.

14 K. Miettunen, X. Ruan, T. Saukkonen, J. Halme, M. Toivola, H. Guangsheng, P. Lund, *Journal of The Electrochemical Society*, 2010, **157**, B814–B819.

15 M. Carnie, D. Bryant, T. Watson, D. Worsley, *Internationa Journar of Photoenergy*, 2012, **2012**, 1–8.

16 N. Kato, Y. Takeda, K. Higuchi, A. Takeichi, E. Sudo, H. Tanaka, T. Motohiro, T. Sano, T. Toyoda, *Solar Energy Materials & Solar Cells*, 2009, **93**, 893–897.

17 G. Xue, Y. Guo, T. Yu, J. Guan, X. Yu, J. Zhang, J. Liu, Z. Zou, *International Journal of Electrochemical Science*, 2012, **7**, 1496–1511.

18 C.-H. Lee, K.-M. Lee, Y.-L. Tung, J.-M. Wu, *Journal of The Electrochemical Society*, 2012, **159**, B430–B433.

19 M. Toivola, L. Peltokorpi, J. Halme, P. Lund, *Solar Energy Materials & Solar Cells*, 2007, **91**, 1733–1742.

20 P.M. Sommeling, M. Späth, H.J.P. Smit, N.J. Bakker, J.M. Kroon, *Journal of Photochemistry and Photobiology A: Chemistry*, 2004, **164**, 137–144.

21 A. Hinsch, J.M. Kroon, R. Kern, I. Uhlendorf, J. Holzbock, A. Mayer, J. Ferber, *Progress in Photovoltaics: Research and Applications*, 2001, **9**, 425–438.

22 M.-J. Kim, N.-G. Park, *Applied Surface Science*, 2012, **258**, 8915–8918.

23 A. Fischer, H. Pettersson, A. Hagfeldt, G. Boschloo, L. Kloo, M. Gorlov, *Solar Energy Materials & Solar Cells*, 2007, **91**, 1062–1065.

24 M. Bokalič, U. Opara Krašovec, M. Topič, *Progress in Photovoltaics: Research and Applications*, 2013, **21**, 1176–1180.

25 U. Opara Krašovec, M. Bokalič, M. Topič, *Solar Energy Materials & Solar Cells*, 2013, **117**, 67–72.

26 A. Hinsch, H. Brandt, W. Veurman, S. Hemming, M. Nittel, U. Würfel, P. Putyra, C. Lang-Koetz, M. Stabe, S. Beucker, K. Fichter, *Solar Energy Materials & Solar Cells*, 2009, **93**, 820–824.

27 U. Opara Krašovec, M. Berginc, M. Hočevar, M. Topič, *Solar Energy Materials & Solar Cells*, 2009, **93**, 379–381.

28 D. Kuang, P. Wang, S. Ito, S.M. Zakeeruddin, M. Grätzel, *Journal of the American Chemical Society*, 2006, **128**, 7732–7733.

29 M. Adachi, M. Sakamoto, J. Jiu, Y. Ogata, S. Isoda, *The Journal of Physical Chemistry B*, 2006, **110**, 13872.

30 S. Mastroianni, A. Lembo, T.M. Brown, A. Reale, A. Di Carlo, *ChemPhysChem: a European journal of chemical physics and physical chemistry*, 2012, **13**, 2964–2975.

31 S. Mastroianni, A. Lanuti, T.M. Brown, R. Argazzi, S. Caramori, A. Reale, A. Di Carlo, *Applied Physics Letters*, 2012, **101**, 123302.

32 E. Figgemeier, A. Hagfeldt, *International Journal of Photoenergy*, 2004, **6**, 127–140.